Cosmic rays: a proxy to study solar transient events

Arun Babu K. P.
iamarunbabu@gmail.com
arun@igeofisica.unam.mx

ICRR Seminars

22 January 2021

Outline

- Introduction
- Forbush Decrease Models
- Relation of FD and Interplanetary MAgnetic field
- Interplanetary Magnetic Flux-rope Observation by HAWC

Outline

- Introduction
- Forbush Decrease Models
- Relation of FD and Interplanetary MAgnetic field
- Interplanetary Magnetic Flux-rope Observation by HAWC

A&A 555, A139 (2013)
DOI: 10.1051/0004-6361/201220830

Astronomy & Astrophysics

High-rigidity Forbush decreases: due to CMEs or shocks?★

K. P. Arunbabu[1], H. M. Antia[2,3], S. R. Dugad[2,3], S. K. Gupta[2,3], Y. Hayashi[4], S. Kawakami[4], P. K. Mohanty[2,3], T. Nonaka[4], A. Oshima[5], and P. Subramanian[1]
(The GRAPES-3 Collaboration)

[1] Indian Institute of Science Education and Research, Sai Trinity Building, Pashan, 411 021 Pune, India
[2] Tata Institute of Fundamental Research, Homi Bhabha Road, 400 005 Mumbai, India
[3] The GRAPES–3 Experiment, Cosmic Ray Laboratory, Raj Bhavan, 643 001 Ooty, India
[4] Graduate School of Science, Osaka City University, 558-8585 Osaka, Japan
[5] National Astronomical Observatory of Japan, CfCA, 181-8588 Tokyo, Japan

Received 2 December 2012 / Accepted 17 April 2013

ABSTRACT

Aims. We seek to identify the primary agents causing Forbush decreases (FDs) in high-rigidity cosmic rays observed from the Earth

Outline

- Introduction
- Forbush Decrease Models
- Relation of FD and Interplanetary MAgnetic field
- Interplanetary Magnetic Flux-rope Observation by HAWC

A&A 580, A41 (2015)
DOI: 10.1051/0004-6361/201425115

Astronomy & Astrophysics

How are Forbush decreases related to interplanetary magnetic field enhancements?★

K. P. Arunbabu[1,2], H. M. Antia[2,3], S. R. Dugad[2,3], S. K. Gupta[2,3], Y. Hayashi[2,4], S. Kawakami[2,4], P. K. Mohanty[2,3], A. Oshima[2,5], and P. Subramanian[1,2]

[1] Indian Institute of Science Education and Research, Dr. Homi Bhabha Road, Pashan, 411 021 Pune, India
e-mail: gupta@grapes.tifr.res.in
[2] The GRAPES–3 Experiment, Cosmic Ray Laboratory, Raj Bhavan, 643 001 Ooty, India
[3] Tata Institute of Fundamental Research, Homi Bhabha Road, Mumbai, Maharashtra, India
[4] Graduate School of Science, Osaka City University, Osaka 558-8585, Japan
[5] College of Engineering, Chubu University, Kasugai, Aichi 487-8501, Japan

Received 6 October 2014 / Accepted 24 April 2015

ABSTRACT

Outline

- Introduction
- Forbush Decrease Models
- Relation of FD and Interplanetary MAgnetic field
- Interplanetary Magnetic Flux-rope Observation by HAWC

THE ASTROPHYSICAL JOURNAL, 905:73 (23pp), 2020 December 10 https://doi.org/10.3847/1538-4357/abc344

CrossMark

Interplanetary Magnetic Flux Rope Observed at Ground Level by HAWC

S. Akiyama[1], R. Alfaro[2], C. Alvarez[3], J. R. Angeles Camacho[2], J. C. Arteaga-Velázquez[4], K. P. Arunbabu[5], D. Avila Rojas[2], H. A. Ayala Solares[6], E. Belmont-Moreno[2], K. S. Caballero-Mora[3], T. Capistrán[7], A. Carramiñana[7], S. Casanova[8], P. Colin-Farias[5,9], U. Cotti[4], J. Cotzomi[10], E. De la Fuente[11], C. de León[4], R. Diaz Hernandez[7], C. Espinoza[2], N. Fraija[12], A. Galván-Gámez[12], D. Garcia[2], J. A. García-González[2], F. Garfias[12], M. M. González[12], J. A. Goodman[13], J. P. Harding[14], B. Hona[15], D. Huang[15], F. Hueyotl-Zahuantitla[3], P. Hüntemeyer[15], A. Iriarte[12], V. Joshi[16], D. Kieda[17], G. J. Kunde[14], A. Lara[5], H. León Vargas[2], G. Luis-Raya[18], K. Malone[14], J. Martínez-Castro[19], J. A. Matthews[20], P. Miranda-Romagnoli[21], E. Moreno[10], A. Nayerhoda[8], L. Nellen[22], M. Newbold[17], T. Niembro[23], T. Nieves-Chinchilla[24], R. Noriega-Papaqui[21], E. G. Pérez-Pérez[18], L. Preisser[5], C. D. Rho[25], J. Ryan[26], H. Salazar[10], F. Salesa Greus[8], A. Sandoval[2], R. W. Springer[17], I. Torres[7], F. Ureña-Mena[7], L. Villaseñor[10], and A. Zepeda[27]

[1] The Catholic University of America, Washington, DC, USA
[2] Instituto de Física, Universidad Nacional Autónoma de México, Ciudad de México, Mexico
[3] Universidad Autónoma de Chiapas, Tuxtla Gutiérrez, Chiapas, Mexico
[4] Universidad Michoacana de San Nicolás de Hidalgo, Morelia, Mexico
[5] Instituto de Geofísica, Universidad Nacional Autónoma de México, Ciudad de México, Mexico; arun@igeofisica.unam.mx, alara@igeofisica.unam.mx
[6] Department of Physics, Pennsylvania State University, University Park, PA, USA
[7] Instituto Nacional de Astrofísica, Óptica y Electrónica, Puebla, Mexico
[8] Institute of Nuclear Physics, Polish Academy of Sciences, PL-31342 IFJ-PAN, Krakow, Poland
[9] Posgrado en Ciencias de la Tierra, Universidad Nacional Autónoma de México, Ciudad de México, Mexico
[10] Facultad de Ciencias Físico Matemáticas, Benemérita Universidad Autónoma de Puebla, Puebla, Mexico

CME

- Coronal Mass Ejections (CMEs) are large blobs of (solar) coronal plasma

CME

- Coronal Mass Ejections (CMEs) are large blobs of (solar) coronal plasma
- CMEs are expelled (together with magnetic fields) and propagate through the interplanetary medium.

CME

- Coronal Mass Ejections (CMEs) are large blobs of (solar) coronal plasma
- CMEs are expelled (together with magnetic fields) and propagate through the interplanetary medium.
- Sometimes CMEs are directed towards Earth and cause geomagnetic storms.

CME

- Coronal Mass Ejections (CMEs) are large blobs of (solar) coronal plasma
- CMEs are expelled (together with magnetic fields) and propagate through the interplanetary medium.
- Sometimes CMEs are directed towards Earth and cause geomagnetic storms.
- We investigate the structure and effects of CMEs using Galactic cosmic rays (GCRs) as a probe

CME

- Coronal Mass Ejections (CMEs) are large blobs of (solar) coronal plasma
- CMEs are expelled (together with magnetic fields) and propagate through the interplanetary medium.
- Sometimes CMEs are directed towards Earth and cause geomagnetic storms.
- We investigate the structure and effects of CMEs using Galactic cosmic rays (GCRs) as a probe

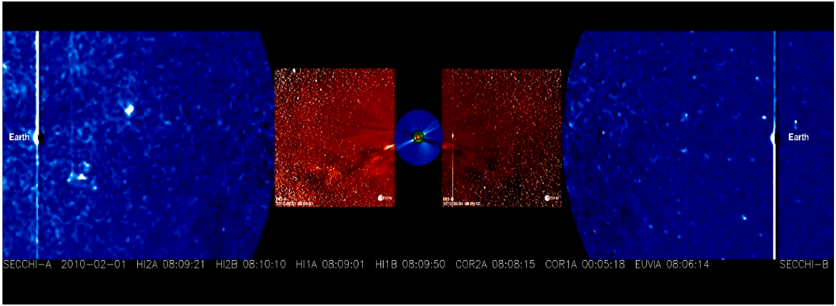

CME, Shock & Sheath

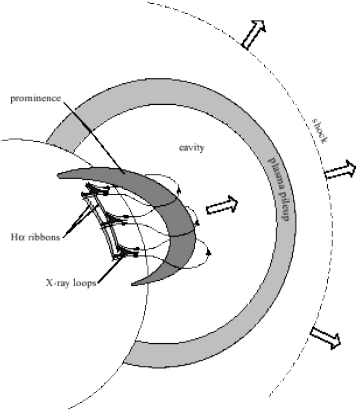

CME, Shock & Sheath

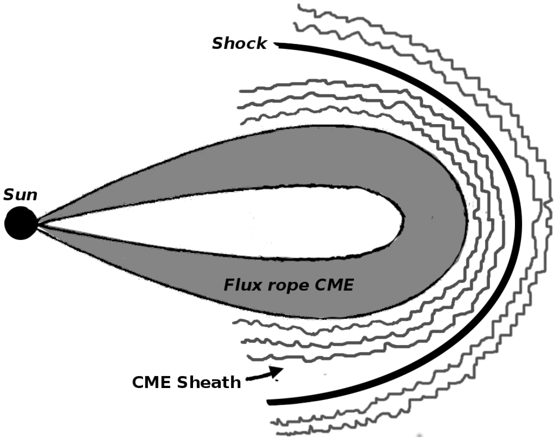

Sun-Earth connection

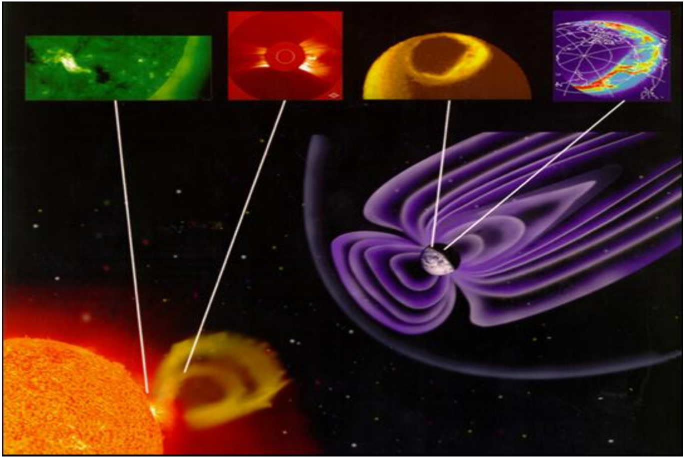

Cosmic rays and Solar activity

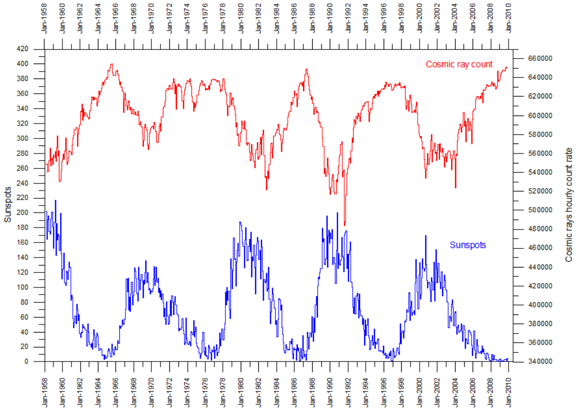

Cosmic rays and Solar activity

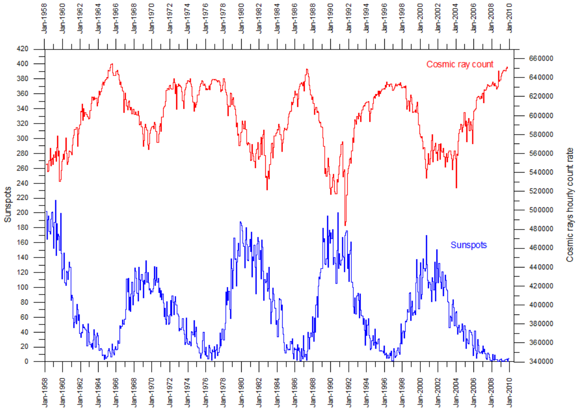

- Being a charged particles, GCRs are profoundly affected by the magnetic fields carried by the solar wind, specially by CME-shock-sheath system.

Cosmic rays and Solar activity

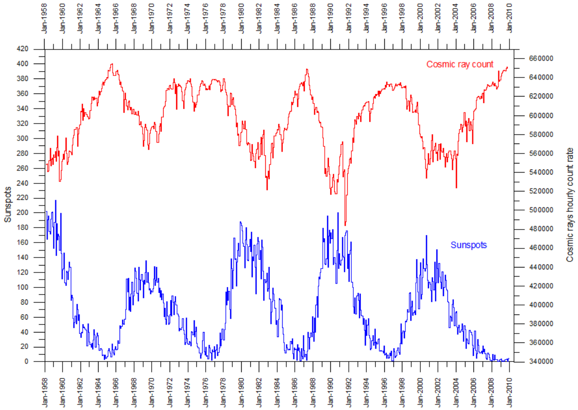

- Being a charged particles, GCRs are profoundly affected by the magnetic fields carried by the solar wind, specially by CME-shock-sheath system.
- Galactic cosmic rays (GCRs) are a good probe to study the Solar Transient Events.

Forbush decrease

Forbush decrease (FD) is a transient decrease in the observed galactic cosmic ray intensity at the Earth.

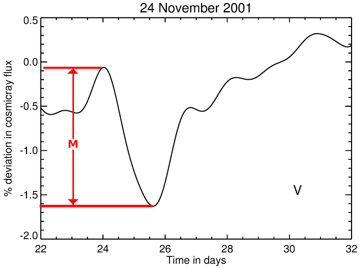

Forbush decrease

Forbush decrease (FD) is a transient decrease in the observed galactic cosmic ray intensity at the Earth.

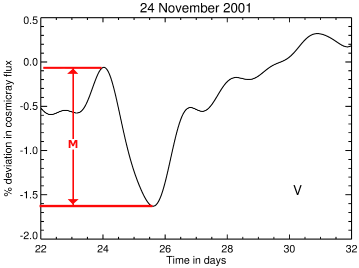

Can be due to magnetic field compression of shock (like an umbrella), or low (cosmic ray) density magnetic cloud behind it.

Forbush decrease

Forbush decrease (FD) is a transient decrease in the observed galactic cosmic ray intensity at the Earth.

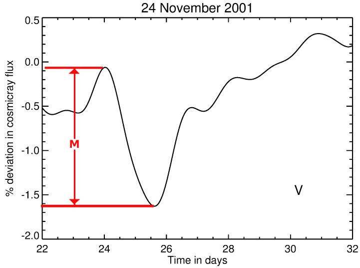

Can be due to magnetic field compression of shock (like an umbrella), or low (cosmic ray) density magnetic cloud behind it.
FD magnitude is estimated as the difference of GCR intensity at the pre-event time to that at the minimum of the decrease.

Forbush decrease

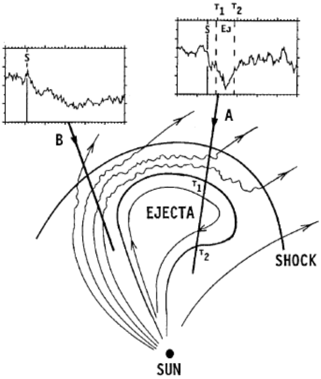

Cane, 2000

Forbush decrease

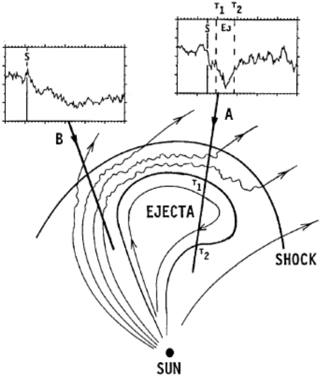

Cane, 2000

- General (theoretical) view: Forbush decrease due to propagating, diffusive barrier; i.e, CME-driven shock
- "Two-step" Forbush decreases! second step due to near-earth CME/magnetic cloud.
- Some attribute entire Forbush decrease is due to the magnetic cloud; i.e, it is a manifestation of the low-density cavity(magnetic cloud) engulfing the earth.

Forbush decrease

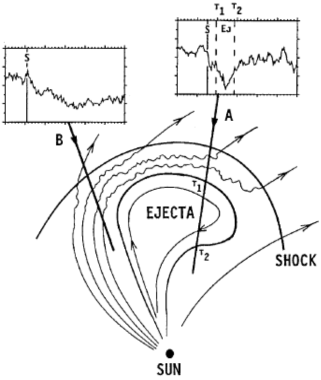

Cane, 2000

- General (theoretical) view: Forbush decrease due to propagating, diffusive barrier; i.e, CME-driven shock
- "Two-step" Forbush decreases! second step due to near-earth CME/magnetic cloud.
- Some attribute entire Forbush decrease is due to the magnetic cloud; i.e, it is a manifestation of the low-density cavity(magnetic cloud) engulfing the earth.

Forbush decrease

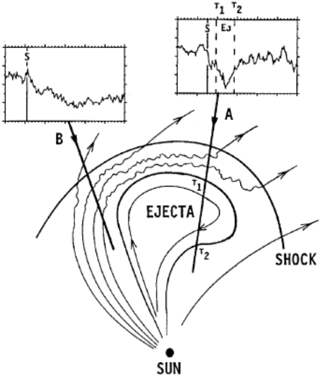

Cane, 2000

- General (theoretical) view: Forbush decrease due to propagating, diffusive barrier; i.e, CME-driven shock
- "Two-step" Forbush decreases! second step due to near-earth CME/magnetic cloud.
- Some attribute entire Forbush decrease is due to the magnetic cloud; i.e, it is a manifestation of the low-density cavity(magnetic cloud) engulfing the earth.

Cut-off Rigidity

- Rigidity $Rg\,(\mathrm{volts}) \equiv P\,c/Z\,e$ indicates how tightly a cosmic ray proton is tied to the magnetic field.

Cut-off Rigidity

- Rigidity $Rg\,(\mathrm{volts}) \equiv P\,c/Z\,e$ indicates how tightly a cosmic ray proton is tied to the magnetic field.
- Protons below the cut-off rigidity don't make it to the top of the atmosphere (to produce a muon shower); they are deflected by the geomagnetic field back into space.

Cut-off Rigidity

- Rigidity $Rg\,(\mathrm{volts}) \equiv P\,c/Z\,e$ indicates how tightly a cosmic ray proton is tied to the magnetic field.
- Protons below the cut-off rigidity don't make it to the top of the atmosphere (to produce a muon shower); they are deflected by the geomagnetic field back into space.
- The cut-off rigidity is very dependent on the B field geometry;

Cut-off Rigidity

- Rigidity $Rg\,(\mathrm{volts}) \equiv P\,c/Z\,e$ indicates how tightly a cosmic ray proton is tied to the magnetic field.
- Protons below the cut-off rigidity don't make it to the top of the atmosphere (to produce a muon shower); they are deflected by the geomagnetic field back into space.
- The cut-off rigidity is very dependent on the B field geometry;

Low ($\rightarrow 0$) for a nearly vertical field, High (*Maximum*) for nearly horizontal field;

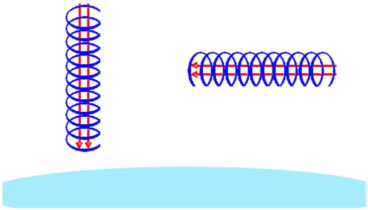

i.e., its dependent on the viewing direction (different for East, West, North, South)

High-rigidity Forbush decreases: due to CMEs or shocks?

- Cosmic ray Forbush decreases are a good proxy to understand the **near-Earth structure of the CME-shock system**.

High-rigidity Forbush decreases: due to CMEs or shocks?

- Cosmic ray Forbush decreases are a good proxy to understand the **near-Earth structure of the CME-shock system**.
- The relative contributions of shocks and coronal mass ejections (CMEs) in causing FDs is a matter of debate.

High-rigidity Forbush decreases: due to CMEs or shocks?

- Cosmic ray Forbush decreases are a good proxy to understand the **near-Earth structure of the CME-shock system**.
- The relative contributions of shocks and coronal mass ejections (CMEs) in causing FDs is a matter of debate.
- We studied the FD events by considering two independant models, and checked the validity of these models using the FD-magnitude to rigidity spectrum from GRAPES-3.
  1. CME-only cumulative diffusion model
  2. Shock-only model

"High-rigidity Forbush decreases: due to CMEs or Shock?", Arunbabu et al., 2013, Astronomy & Astrophysics, 555, 139

GRAPES-3 tracking muon telescope

GRAPES-3 tracking muon telescope

- Located at Ooty, India

GRAPES-3 tracking muon telescope

- Located at Ooty, India
- 11.4^ON, 76.7^OE, at an altitude of 2200 m.

GRAPES-3 tracking muon telescope

- Located at Ooty, India
- 11.4^{O}N, 76.7^{O}E, at an altitude of 2200 m.
- 3712 propotional counters in 4 muon stations each contain 4 modules

GRAPES-3 tracking muon telescope

- Located at Ooty, India
- 11.4^{O}N, 76.7^{O}E, at an altitude of 2200 m.
- 3712 propotional counters in 4 muon stations each contain 4 modules
- Total area 560 m^2, (Now, expansion is doubling this area)

GRAPES-3 tracking muon telescope

- Located at Ooty, India
- 11.4^ON, 76.7^OE, at an altitude of 2200 m.
- 3712 propotional counters in 4 muon stations each contain 4 modules
- Total area 560 m^2, (Now, expansion is doubling this area)
- Cut-off rigidty 15-23.5 GV.

GRAPES-3 tracking muon telescope

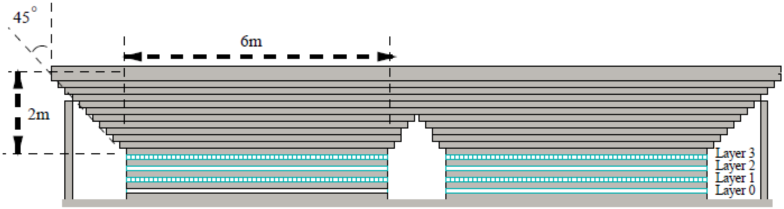

GRAPES-3 tracking muon telescope

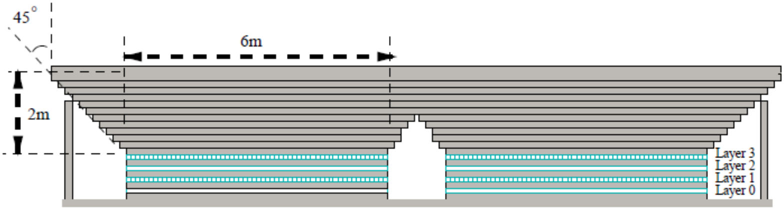

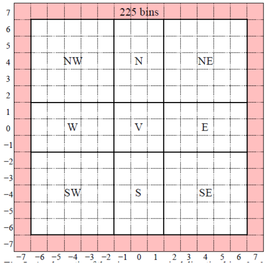

The CME-only model: cumulative diffusion

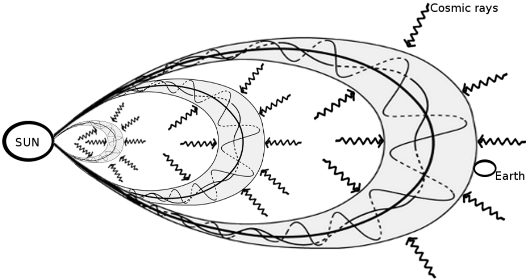

High energy galactic (*not of solar origin*) cosmic rays progressively diffuse into the expanding, propagating CME bubble, across the B fields bounding it.

The CME-only model: cumulative diffusion

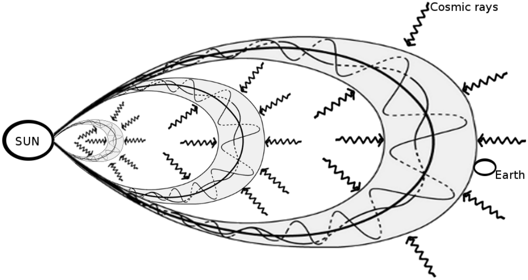

High energy galactic (*not of solar origin*) cosmic rays progressively diffuse into the expanding, propagating CME bubble, across the B fields bounding it.
At the earth, the density contrast between the CME interior & outside (in high energy CR protons) is manifested as the Forbush decrease.

The CME-only model: details

CME-only model

Flux of protons entering CME is

$$F\,(\mathrm{cm}^{-2}\,\mathrm{s}^{-1}) = D_{\perp}(\rho\,,\sigma^2)\,\frac{\partial N_a}{\partial r}$$

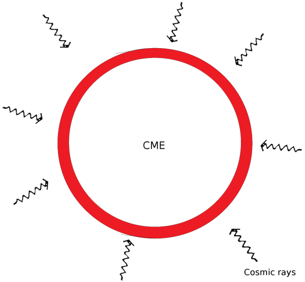

The CME-only model: details

CME-only model

Flux of protons entering CME is

$$F\,(\mathrm{cm^{-2}\,s^{-1}}) = D_{\perp}(\rho\,,\sigma^2)\,\frac{\partial N_a}{\partial r}$$

where

- We used a TWO step velocity profile, first from observation in LASCO field of view, second we assume that CME dynamics are governed exclusively by the aerodynamic drag it experiences due to momentum coupling with the ambient solar wind.
- We assumed the density gradient, which are broadly consistent with observation , (De Simone et al., 2011)

CME-only Model: cumulative diffusion

FD magnitude

$$\mathrm{M} \equiv \frac{N_a - N_i}{N_a} \equiv \frac{\delta N}{N_a}$$

$$\equiv 1 - \frac{2\int_0^T \frac{L(t)R(t)\mathrm{D}_\perp}{\kappa(t)R_L{}^{0.33}}\,dt}{R(T)^2 L(T)}$$

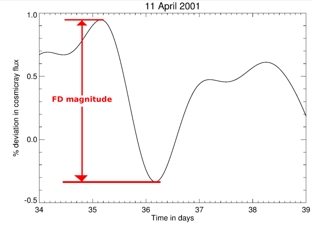

CME-only Model: cumulative diffusion

FD magnitude

$$\mathrm{M} \equiv \frac{N_a - N_i}{N_a} \equiv \frac{\delta N}{N_a}$$

$$\equiv 1 - \frac{2\int_0^T \frac{L(t)R(t)\mathrm{D}_\perp}{\kappa(t){R_L}^{0.33}}\,dt}{R(T)^2 L(T)}$$

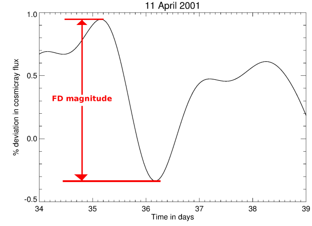

M	:	predicted FD magnitude
$D_\perp$	:	diffusion coefficient $\perp$ large scale B field
R	:	MC radius
L	:	MC length (into sky plane)
R_L	:	Larmor radius

The shock-only model (following Wibberenz et al 1998)

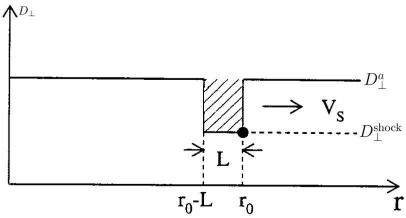

The Forbush decrease is due to the shock - a propagating, diffusive barrier. The B field enhancement at the shock acts as an "umbrella" against galactic cosmic rays.

FD magnitude

$$\mathrm{M} \equiv \frac{\mathrm{U_a - U_{shock}}}{\mathrm{U_a}} = \frac{\Delta \mathrm{U}}{\mathrm{U_a}} = \frac{\mathrm{V_{sw} L_{shock}}}{\mathrm{D_\perp{}^a}} \left(\frac{\mathrm{D_\perp{}^a}}{\mathrm{D_\perp{}^{shock}}} - 1 \right)$$

24 November 2001

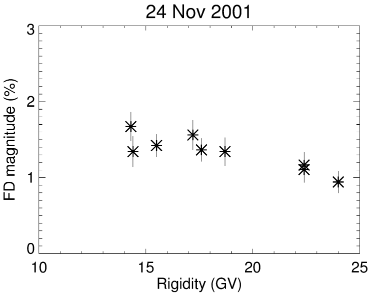

24 November 2001

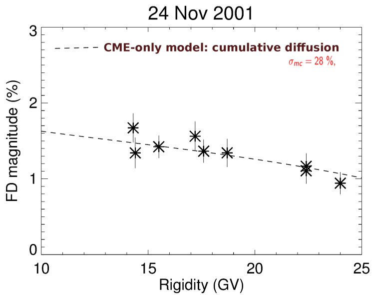

$\sigma^2 \equiv \langle B_{\rm turb}^2 / B_0^2 \rangle$

For CME-only (cumulative diffusion) model, $\sigma_{mc} = 28$ %,
while for shock-only model, $\sigma_{\rm shock} = 400$ %.
Typical quiet sun turbulence level: $\sigma \approx$ 6–15 % (Spangler 2002, Bavassano & Bruno 1995).

24 November 2001

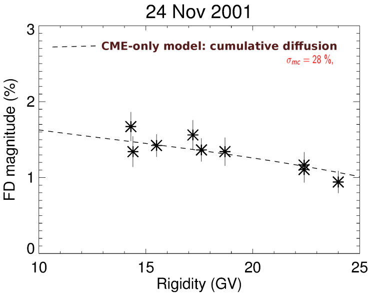

$\sigma^2 \equiv \langle B_{\mathrm{turb}}^2 / B_0^2 \rangle$

For CME-only (cumulative diffusion) model, $\sigma_{mc} = 28$ %,
while for shock-only model, $\sigma_{\mathrm{shock}} = 400$ %.
Typical quiet sun turbulence level: $\sigma \approx$ 6–15 % (Spangler 2002, Bavassano & Bruno 1995).

Forbush decrease due to **cumulative diffusion of protons into the CME through the turbulent sheath is a more reasonable picture**

Results

Event	CME-only model $\sigma_{\rm mc}$	shock-only model $\sigma_{\rm shock}$
11 April 2001	9.4 %	100 %
17 August 2001	13 %	180 %
24 November 2001	28 %	400 %
7 September 2002	13%	100%
20 November 2003	6.7 %	400 %
26 July 2004	46 %	200 %

FDs involving protons of rigidities ranging from 14 to 24 GV, the CME-only model is a viable one, while the shock-only model is not.

How are FDs related with IP mag-field enhancements?

Correlation between FD profile and interplanetary magnetic field enhancement: **understanding cross-field diffusion**

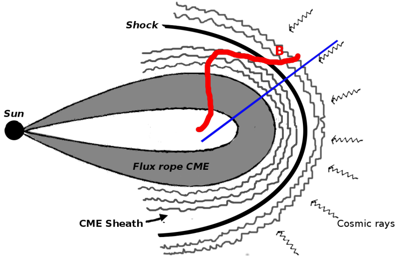

"How are Forbush decreases related with IP magnetic field enhancements ?", K.P. Arunbabu et. al., 2015, Astronomy & Astrophysics, 580, 41

Forbush decrease & IP magnetic field

The shapes of FD profile and IP magnetic field compression are remarkably similar.

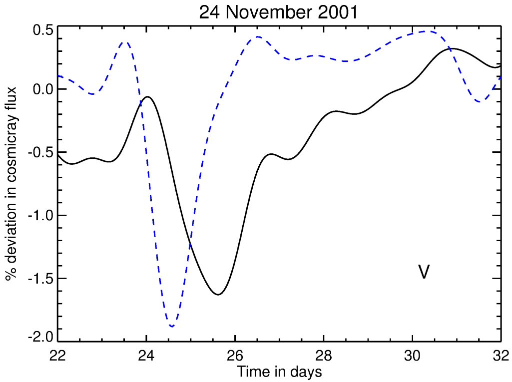

The FD looks like a lagged copy of the B field compression.

IP Magnetic fields

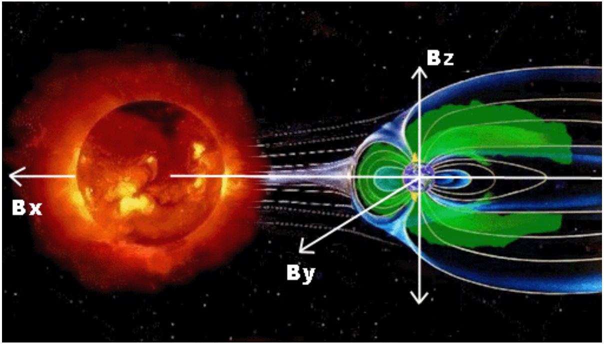

- B_{total}, scalar magnetic field

IP Magnetic fields

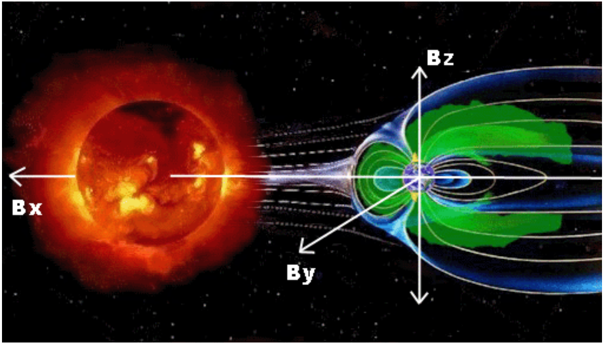

- B_{total}, scalar magnetic field
- B_x, is the magnetic field in the Sun-Earth line in the ecliptic plane and pointing towards Sun

IP Magnetic fields

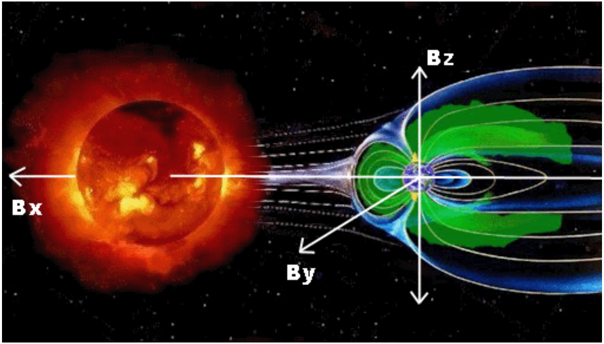

- B_{total}, scalar magnetic field
- B_x, is the magnetic field in the Sun-Earth line in the ecliptic plane and pointing towards Sun
- B_z, is the magnetic field parallel to the ecliptic north pole

IP Magnetic fields

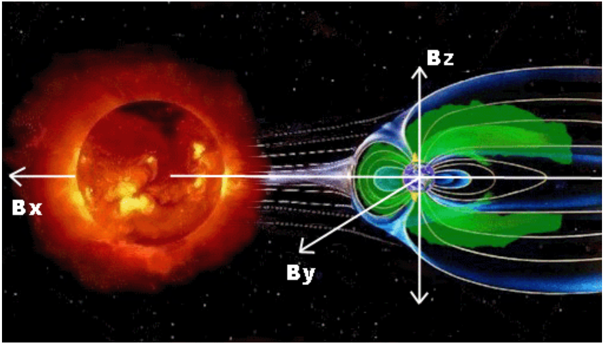

- B_{total}, scalar magnetic field
- B_x, is the magnetic field in the Sun-Earth line in the ecliptic plane and pointing towards Sun
- B_z, is the magnetic field parallel to the ecliptic north pole
- B_y, is the magnetic field in the ecliptic plane pointing towards dusk (opposite the Earth's motion)

IP Magnetic fields

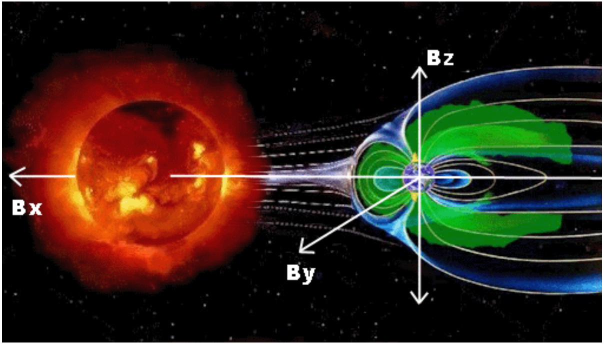

- B_{total}, scalar magnetic field
- B_x, is the magnetic field in the Sun-Earth line in the ecliptic plane and pointing towards Sun
- B_z, is the magnetic field parallel to the ecliptic north pole
- B_y, is the magnetic field in the ecliptic plane pointing towards dusk (opposite the Earth's motion)
- $B_\perp = (B_y^2 + B_z^2)^{0.5}$, perpendicular magnetic field.

Correlation of FD magnitude with B

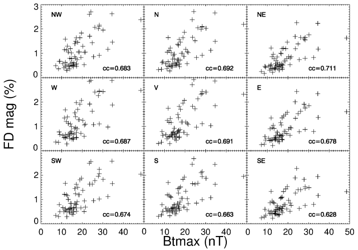

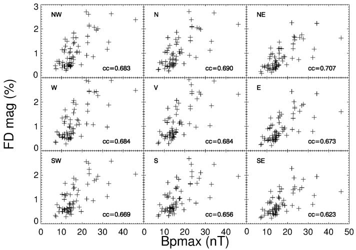

Dir	Corr. with B_{tot}	Corr. with $B_{\perp}$
NW	0.682874	0.682926
N	0.692284	0.689747
NE	0.710686	0.706913
W	0.687189	0.684261
V	0.690613	0.683616
E	0.677899	0.672830
SW	0.674214	0.669421
S	0.662859	0.656359
SE	0.628104	0.622673

B-field compression and Turbulence

B-Field Compression

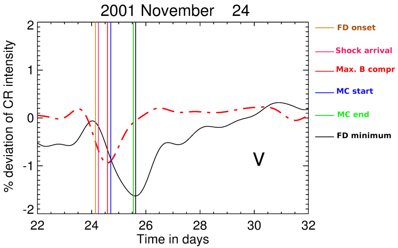

Turbulence Level $\sigma^2 \equiv \langle B^2_{\mathrm{turb}}/B^2_0 \rangle$

B-field compression and Turbulence

B-Field Compression

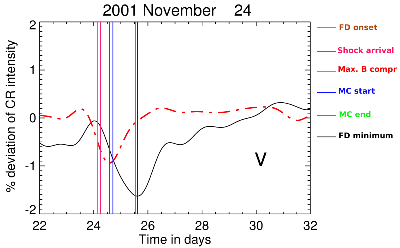

Turbulence Level $\sigma^2 \equiv \langle B^2_{\mathrm{turb}}/B^2_0 \rangle$

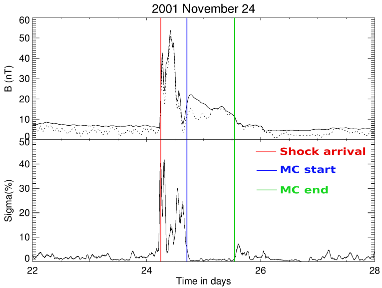

- Enhancement of magnetic field compression responsible for the FD is in fact the **shock sheath**: the region between the shock and the magnetic cloud.

B-field compression and Turbulence

B-Field Compression

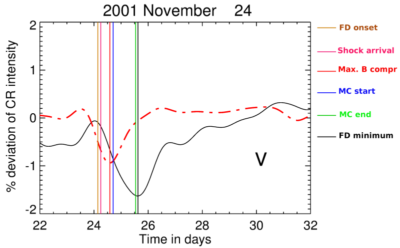

Turbulence Level $\sigma^2 \equiv \langle B^2_{\rm turb}/B^2_0 \rangle$

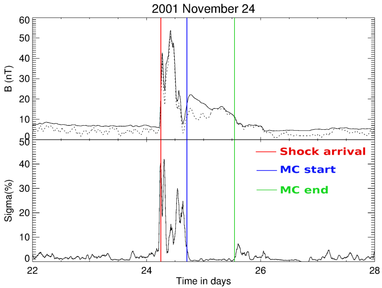

- Enhancement of magnetic field compression responsible for the FD is in fact the **shock sheath**: the region between the shock and the magnetic cloud.
- The turbulence level is also enhanced in the shock sheath.

The FD profile is very similar to the B field compression!

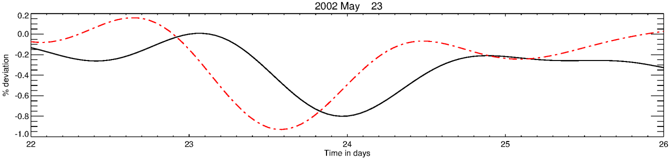

The FD profile is very similar to the B field compression!

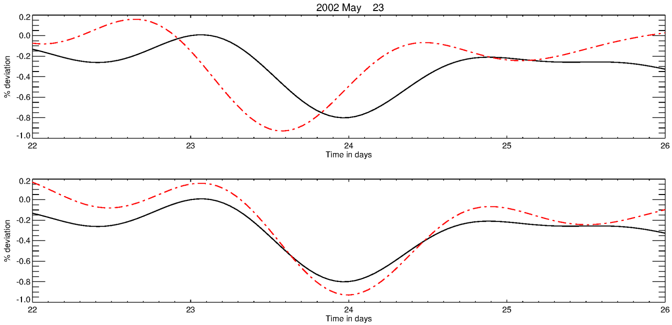

The FD profile is very similar to the B field compression!

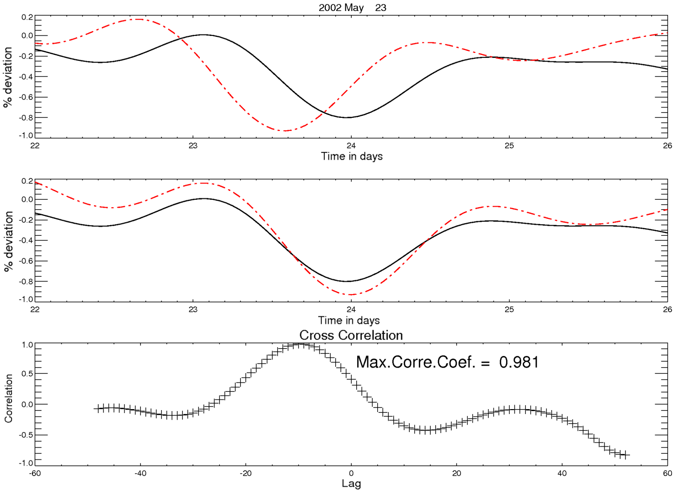

Cross-field diffusion

- We consider the (local) diffusion of high energy protons through the large scale B field compression.

Cross-field diffusion

- We consider the (local) diffusion of high energy protons through the large scale B field compression.
- The lag between the IP mag. field compression and the FD profile can be attributed to (turbulent) cross-field diffusion of protons through the B field compression.

Cross-field diffusion

- We consider the (local) diffusion of high energy protons through the large scale B field compression.
- The lag between the IP mag. field compression and the FD profile can be attributed to (turbulent) cross-field diffusion of protons through the B field compression.
- We calculated the No. of diff. required to address this lag

Cross-field diffusion

- We consider the (local) diffusion of high energy protons through the large scale B field compression.
- The lag between the IP mag. field compression and the FD profile can be attributed to (turbulent) cross-field diffusion of protons through the B field compression.
- We calculated the No. of diff. required to address this lag

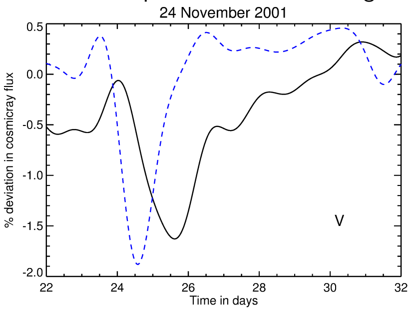

Cross-field diffusion

- We consider the (local) diffusion of high energy protons through the large scale B field compression.
- The lag between the IP mag. field compression and the FD profile can be attributed to (turbulent) cross-field diffusion of protons through the B field compression.
- We calculated the No. of diff. required to address this lag

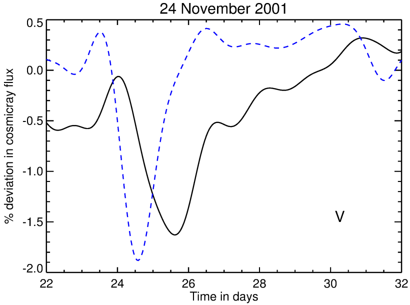

- The FD profile correlates well with the IP magnetic field enhancement profile.

Cross-field diffusion

- We consider the (local) diffusion of high energy protons through the large scale B field compression.
- The lag between the IP mag. field compression and the FD profile can be attributed to (turbulent) cross-field diffusion of protons through the B field compression.
- We calculated the No. of diff. required to address this lag

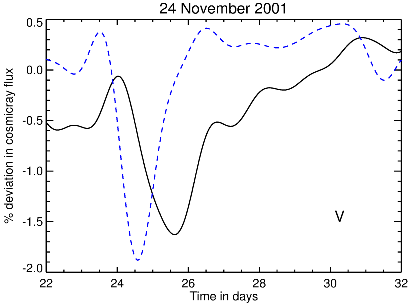

- The FD profile correlates well with the IP magnetic field enhancement profile.
- The observed lag between the FD and the IP magnetic field compression ≈ few tens to few hundred diffusion times.

MFR observation by HAWC

Identification of a magnetic flux-rope, first time using a ground based observatory

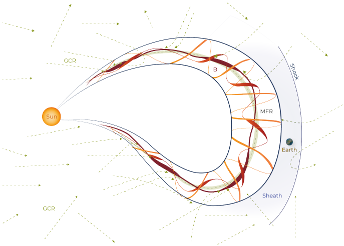

"Interplanetary Magnetic Flux Rope Observed at Ground Level by HAWC", S. Akiyama et al., 2020 The Astrophysical Journal, 905, 73

HAWC

- Located on a plateau between Sierra Negra & Pico de Orizaba volcanoes in Mexico

HAWC

- Located on a plateau between Sierra Negra & Pico de Orizaba volcanoes in Mexico
- $18^{O}59'41"$N, $97^{O}18'30"$W, at an altitude of 4100 m.

HAWC

- Located on a plateau between Sierra Negra & Pico de Orizaba volcanoes in Mexico
- $18^{O}59'41"$N, $97^{O}18'30"$W, at an altitude of 4100 m.
- 300 Water Cherenkov detectors, Each of them 7.3 m diamter and 4.5 m deep.

HAWC

- Located on a plateau between Sierra Negra & Pico de Orizaba volcanoes in Mexico
- $18^{O}59'41''$N, $97^{O}18'30''$W, at an altitude of 4100 m.
- 300 Water Cherenkov detectors, Each of them 7.3 m diamter and 4.5 m deep.
- Span over 22000 m^2 area.

TDC scaler system

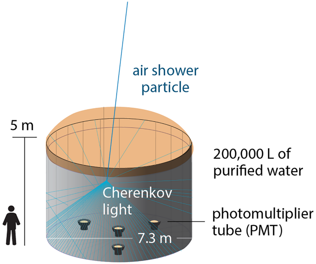

- 4 PMTs, 10" PMT at center and 8" at equilateral triangle of side 3.2 m.

TDC scaler system

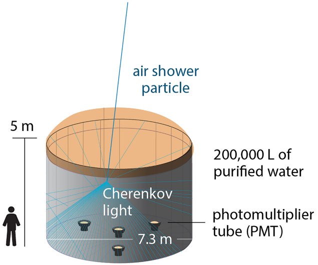

- 4 PMTs, 10" PMT at center and 8" at equilateral triangle of side 3.2 m.
- TDC DAQ counts hits in a time window of 30 ns for each PMT

TDC scaler system

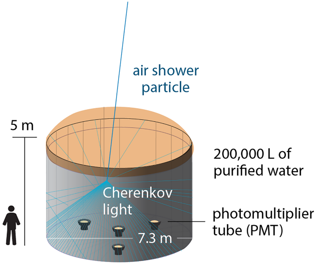

- 4 PMTs, 10" PMT at center and 8" at equilateral triangle of side 3.2 m.
- TDC DAQ counts hits in a time window of 30 ns for each PMT
- Single PMT rate and multiplicity M2, M3, M4 are recorded.

TDC scaler system

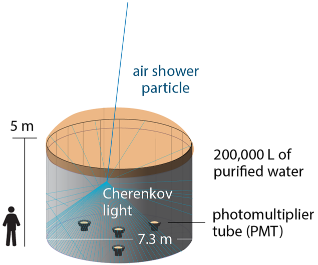

- 4 PMTs, 10" PMT at center and 8" at equilateral triangle of side 3.2 m.
- TDC DAQ counts hits in a time window of 30 ns for each PMT
- Single PMT rate and multiplicity M2, M3, M4 are recorded.
- Cut-off rigidity 8GV and median rigidity 40-46 GV.

TDC scaler system

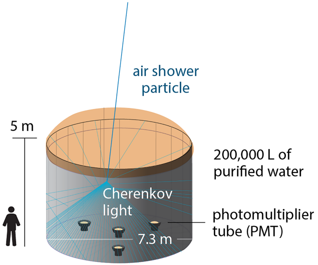

- 4 PMTs, 10" PMT at center and 8" at equilateral triangle of side 3.2 m.
- TDC DAQ counts hits in a time window of 30 ns for each PMT
- Single PMT rate and multiplicity M2, M3, M4 are recorded.
- Cut-off rigidity 8GV and median rigidity 40-46 GV.
- Can measure GCR intensity with accuracy $< 0.01\%$ for every minute.

Solar modulations

Parker's Transport equation

$$\frac{\partial n}{\partial t} + V_{sw} \cdot \bigtriangledown n - \bigtriangledown \cdot (\kappa \cdot \bigtriangledown n) - \frac{1}{3}(\bigtriangledown \cdot V_{sw})\frac{\partial n}{\partial ln\ p} = S$$

- The GCR intensity can be considered to be in quasi-equilibrium, hence the source term S and rate of change of the GCR density $\frac{\partial n}{\partial t}$ can be ignored.

Solar modulations

Parker's Transport equation

$$\frac{\partial n}{\partial t} + V_{sw} \cdot \bigtriangledown n - \bigtriangledown \cdot (\kappa \cdot \bigtriangledown n) - \frac{1}{3}(\bigtriangledown \cdot V_{sw})\frac{\partial n}{\partial ln\ p} = S$$

- The GCR intensity can be considered to be in quasi-equilibrium, hence the source term S and rate of change of the GCR density $\frac{\partial n}{\partial t}$ can be ignored.
- By numerically solving the Fokker-Planck equation, it was shown that effect of the adiabatic cooling becomes very small at rigidities > 10 GV . Thus, the adiabatic term $\frac{1}{3}(\nabla . V_{SW})\frac{\partial n}{\partial ln\ P}$ can also be ignored.

Solar modulations

Parker's Transport equation

$$\frac{\partial n}{\partial t} + V_{sw} \cdot \bigtriangledown n - \bigtriangledown \cdot (\kappa \cdot \bigtriangledown n) - \frac{1}{3}(\bigtriangledown \cdot V_{sw})\frac{\partial n}{\partial ln\ p} = S$$

- The GCR intensity can be considered to be in quasi-equilibrium, hence the source term S and rate of change of the GCR density $\frac{\partial n}{\partial t}$ can be ignored.
- By numerically solving the Fokker-Planck equation, it was shown that effect of the adiabatic cooling becomes very small at rigidities $>$ 10 GV . Thus, the adiabatic term $\frac{1}{3}(\nabla . V_{SW})\frac{\partial n}{\partial ln\ P}$ can also be ignored.
- The lowest-order approximation of the transport equation is the diffusion-convection framework.

Solar modulations

Parker's Transport equation

$$\frac{\partial n}{\partial t} + V_{sw} \cdot \bigtriangledown n - \bigtriangledown \cdot (\kappa \cdot \bigtriangledown n) - \frac{1}{3}(\bigtriangledown \cdot V_{sw})\frac{\partial n}{\partial ln\ p} = S$$

- The GCR intensity can be considered to be in quasi-equilibrium, hence the source term S and rate of change of the GCR density $\frac{\partial n}{\partial t}$ can be ignored.
- By numerically solving the Fokker-Planck equation, it was shown that effect of the adiabatic cooling becomes very small at rigidities > 10 GV . Thus, the adiabatic term $\frac{1}{3}(\nabla . V_{SW})\frac{\partial n}{\partial ln\ P}$ can also be ignored.
- The lowest-order approximation of the transport equation is the diffusion-convection framework.
- This inward diffusive flux is countered by an outward convective flux, Vn - $\kappa\frac{dn}{dr} = 0$

Solar modulations

Parker's Transport equation

$$\frac{\partial n}{\partial t} + V_{sw} \cdot \bigtriangledown n - \bigtriangledown \cdot (\kappa \cdot \bigtriangledown n) - \frac{1}{3}(\bigtriangledown \cdot V_{sw})\frac{\partial n}{\partial ln\ p} = S$$

- The GCR intensity can be considered to be in quasi-equilibrium, hence the source term S and rate of change of the GCR density $\frac{\partial n}{\partial t}$ can be ignored.
- By numerically solving the Fokker-Planck equation, it was shown that effect of the adiabatic cooling becomes very small at rigidities $>$ 10 GV . Thus, the adiabatic term $\frac{1}{3}(\nabla . V_{SW})\frac{\partial n}{\partial ln\ P}$ can also be ignored.
- The lowest-order approximation of the transport equation is the diffusion-convection framework.
- This inward diffusive flux is countered by an outward convective flux, Vn - $\kappa\frac{dn}{dr}$ $= 0$
- where κ depends on magnetic field B, turbulence level and rigidity of particle.
- Our observations will have modulation effects, due to variation in velocity V and magnetic field B

TDC Scaler Rate

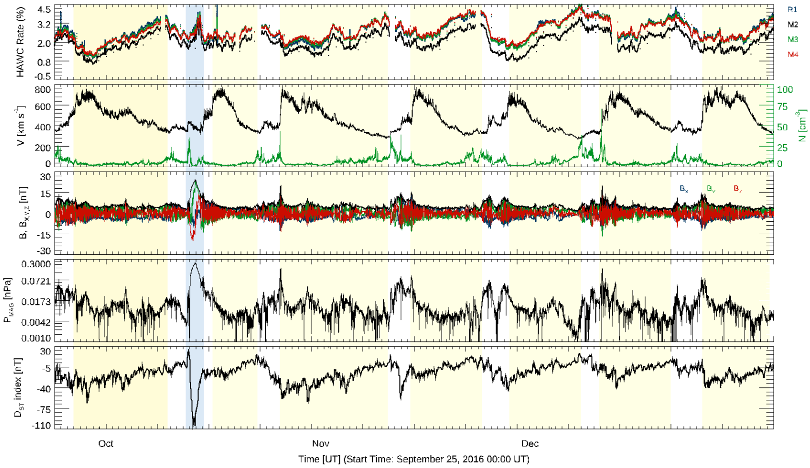

TDC Scaler Rate-Local

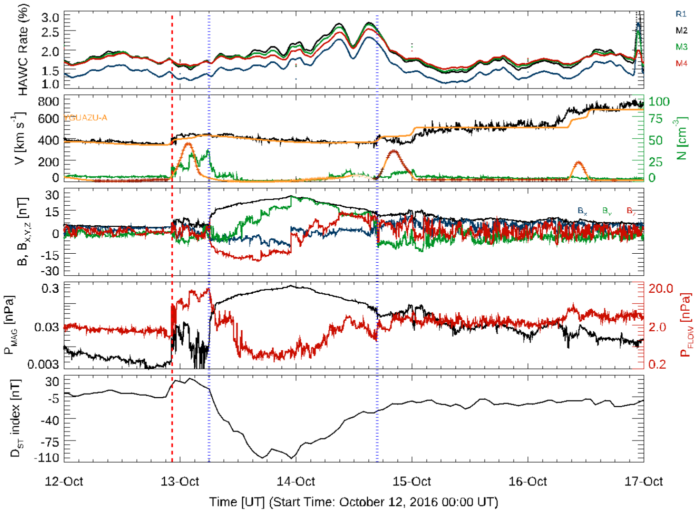

Significance of Event in HAWC observation

Distribution of standard deviation of HAWC TDC-scaler rate

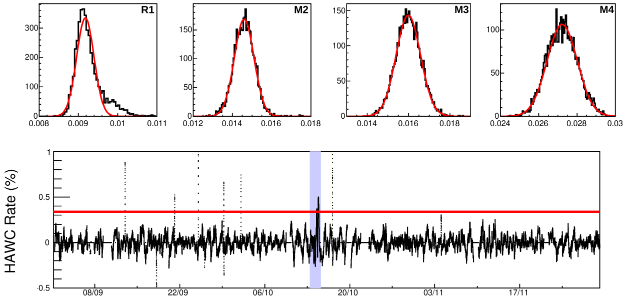

Time [UT] (Start time : September 1, 2016 00:00 UT)

Significance of Event in HAWC observation

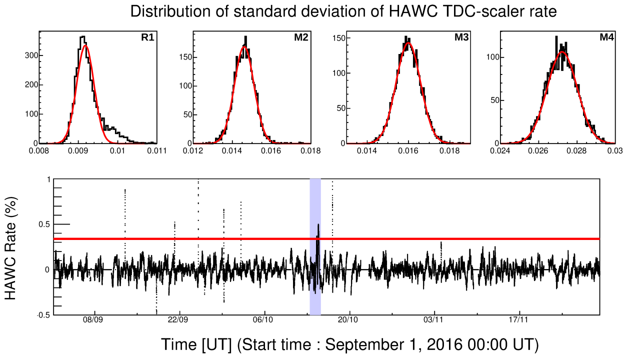

TDC-Scaler	σ (%)	Magnitude of Peak 1 (%)	Magnitude of Peak 1 in terms of σ	Magnitude of Peak 2 (%)	Magnitude of Peak 2 in terms of σ
R_1	9.18×10^{-03}	0.7122	77.6	0.7761	84.6
M_2	1.46×10^{-02}	0.7562	51.8	0.7843	53.7
M_3	1.60×10^{-02}	0.7235	45.2	0.7940	49.7
M_4	2.72×10^{-02}	0.6690	24.6	0.7570	27.8

First thought

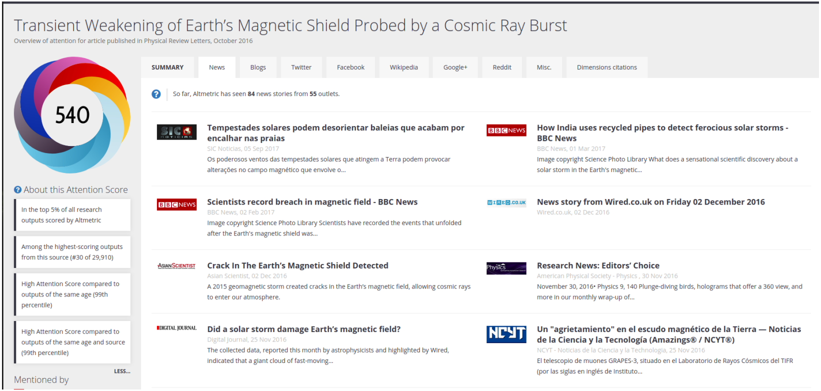

Transcient Weakening of Earth's Magnetic Shield Probed by a Cosmic Ray Burst

Overview of attention for article published in Physical Review Letters, October 2016

540

About this Attention Score

In the top 5% of all research outputs scored by Altmetric

Among the highest-scoring outputs from this source (#30 of 29,910)

High Attention Score compared to outputs of the same age (99th percentile)

High Attention Score compared to outputs of the same age and source (99th percentile)

LESS...

Mentioned by

SUMMARY | News | Blogs | Twitter | Facebook | Wikipedia | Google+ | Reddit | Misc. | Dimensions citations

So far, Altmetric has seen **84** news stories from **55** outlets.

Tempestades solares podem desorientar baleias que acabam por encalhar nas praias
SIC Noticias, 05 Sep 2017
Os poderosos ventos das tempestades solares que atingem a Terra podem provocar alterações no campo magnético que envolve o...

How India uses recycled pipes to detect ferocious solar storms - BBC News
BBC News, 01 Mar 2017
Image copyright Science Photo Library What does a sensational scientific discovery about a solar storm in the Earth's magnetic...

Scientists record breach in magnetic field - BBC News
BBC News, 02 Feb 2017
Image copyright Science Photo Library Scientists have recorded the events that unfolded after the Earth's magnetic shield was...

News story from Wired.co.uk on Friday 02 December 2016
Wired.co.uk, 02 Dec 2016

Crack In The Earth's Magnetic Shield Detected
Asian Scientist, 02 Dec 2016
A 2015 geomagnetic storm created cracks in the Earth's magnetic field, allowing cosmic rays to enter our atmosphere.

Research News: Editors' Choice
American Physical Society - Physics , 30 Nov 2016
November 30, 2016• Physics 9, 140 Plunge-diving birds, holograms that offer a 360 view, and more in our monthly wrap-up of...

Did a solar storm damage Earth's magnetic field?
Digital Journal, 25 Nov 2016
The collected data, reported this month by astrophysicists and highlighted by Wired, indicated that a giant cloud of fast-moving...

Un "agrietamiento" en el escudo magnético de la Tierra — Noticias de la Ciencia y la Tecnología (Amazings® / NCYT®)
NCYT - Noticias de la Ciencia y la Technologia, 25 Nov 2016
El telescopio de muones GRAPES-3, situado en el Laboratorio de Rayos Cósmicos del TIFR (por las siglas en inglés de Instituto...

But this event was not due to these analogy

CME transport

Using a 2D hydrodynamic code we are able to reproduce the speed and density SW profiles observed at 1AU before, during and after the passage of the ICME

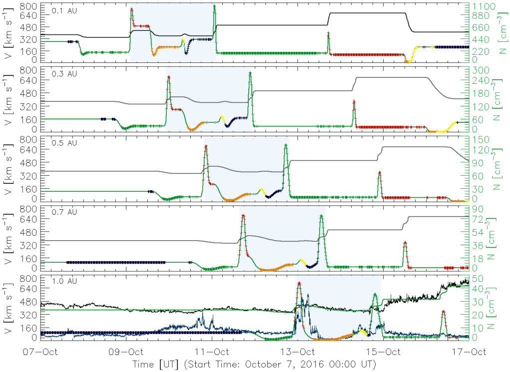

In this particular event the CME/magnetic-cloud/flux-rope was not perturbed by other SW structures in the interplanetary medium

Effects on magnetosphere

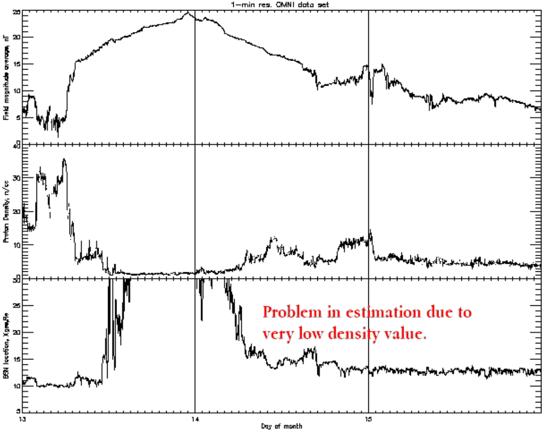

Effects on magnetosphere

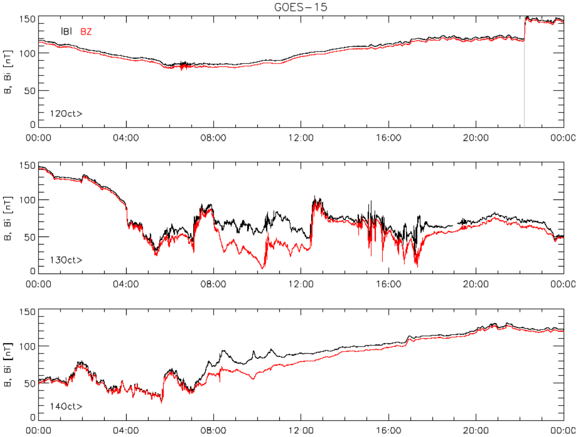

Also time of event was not correlating with the magnetosphere disturbances.

What can be the cause?

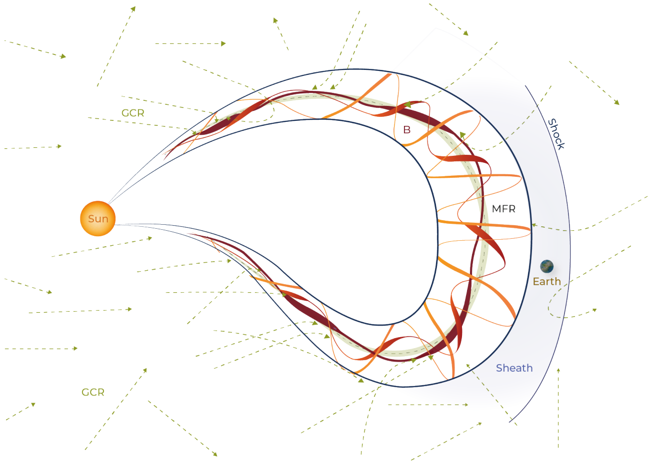

Flux-rope

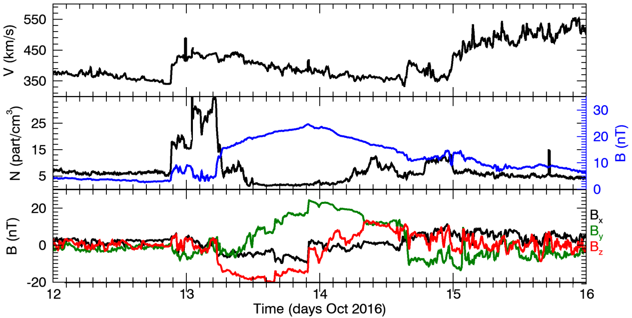

- We fitted the fluxrope model in circular cylindrical coordinate system (Nieves-Chinchilla et al. 2019)

Flux-rope

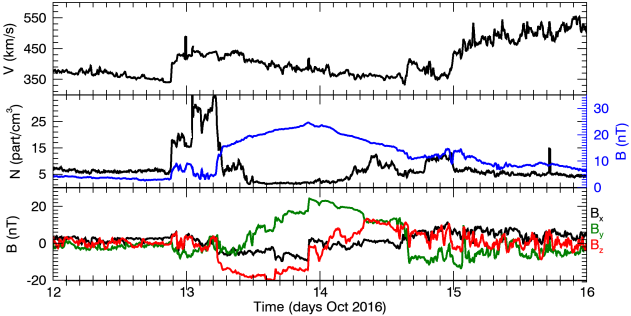

- We fitted the fluxrope model in circular cylindrical coordinate system (Nieves-Chinchilla et al. 2019)
- $B_r \;=\; 0, \qquad B_y \;=\; B_y^0\left[1-\left(\frac{r}{R}\right)^2\right], \qquad B_\phi \;=\; -H\frac{B_y^0}{|C_{10}|}\frac{r}{R},$

Flux-rope

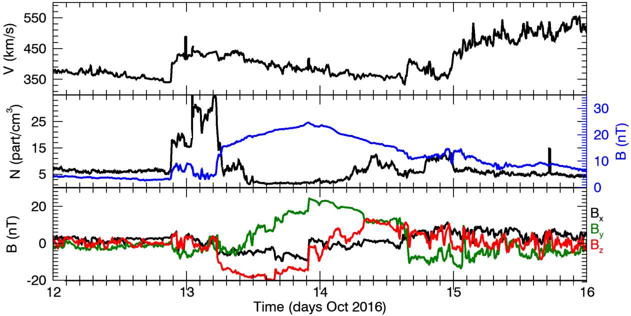

- We fitted the fluxrope model in circular cylindrical coordinate system (Nieves-Chinchilla et al. 2019)
- $B_r = 0, \qquad B_y = B_y^0\left[1-\left(\frac{r}{R}\right)^2\right], \qquad B_\phi = -H\frac{B_y^0}{|C_{10}|}\frac{r}{R},$
- MFR was having an axis orientation of longitude $\phi = 99^O$ and latitude $\theta = -21^O$.

Flux-rope

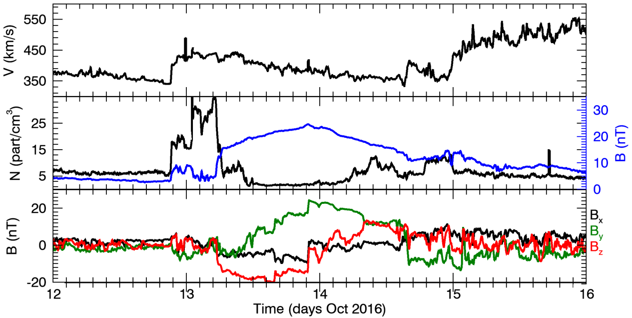

- We fitted the fluxrope model in circular cylindrical coordinate system (Nieves-Chinchilla et al. 2019)
- $B_r = 0, \qquad B_y = B_y^0\left[1-\left(\frac{r}{R}\right)^2\right], \qquad B_\phi = -H\frac{B_y^0}{|C_{10}|}\frac{r}{R},$
- MFR was having an axis orientation of longitude $\phi = 99^O$ and latitude $\theta = -21^O$.
- Radius of fluxrope were 0.146 AU.

Validating GCR guiding

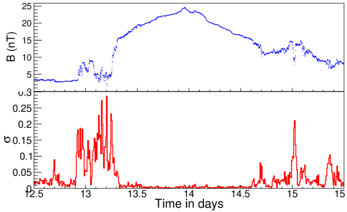

Validating GCR guiding

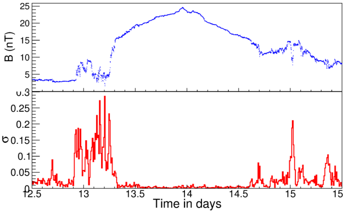

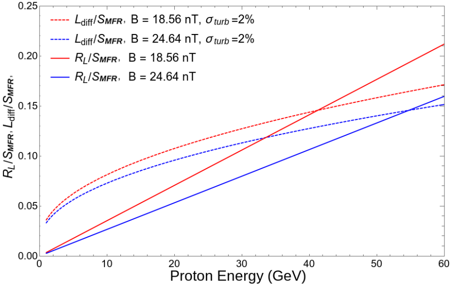

- Low turbulene level make it feasible for Lorentz acceleration.

Validating GCR guiding

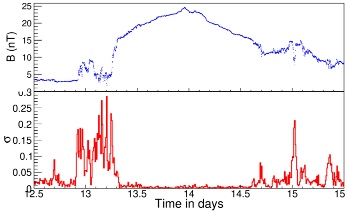

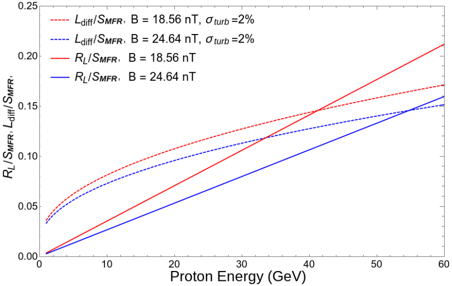

- Low turbulene level make it feasible for Lorentz acceleration.
- Larmor radius and diffusion length are $<<$ than size of MFR

Simulation of Particle Trajectory

- We used Cordinate system with origin at MFR center.

Simulation of Particle Trajectory

- We used Cordinate system with origin at MFR center.
- It can be obtained from GSE by rotation R_Z by θ and R_Y by ϕ.

Simulation of Particle Trajectory

- We used Cordinate system with origin at MFR center.
- It can be obtained from GSE by rotation R_Z by θ and R_Y by ϕ.
- Then assumed the MFR have cylindrical crosssection

Simulation of Particle Trajectory

- We used Cordinate system with origin at MFR center.
- It can be obtained from GSE by rotation R_Z by θ and R_Y by ϕ.
- Then assumed the MFR have cylindrical crosssection
- Field inside MFR were modelled using observations at 1 AU.

Simulation of Particle Trajectory

- We used Cordinate system with origin at MFR center.
- It can be obtained from GSE by rotation R_Z by θ and R_Y by ϕ.
- Then assumed the MFR have cylindrical crosssection
- Field inside MFR were modelled using observations at 1 AU.
- Accelerations were estimated using Lorentz force

Simulation of Particle Trajectory

- We used Cordinate system with origin at MFR center.
- It can be obtained from GSE by rotation R_Z by θ and R_Y by ϕ.
- Then assumed the MFR have cylindrical crosssection
- Field inside MFR were modelled using observations at 1 AU.
- Accelerations were estimated using Lorentz force
- Relativistic converson were used into particle frame.

Simulation of Particle Trajectory

- We used Cordinate system with origin at MFR center.
- It can be obtained from GSE by rotation R_Z by θ and R_Y by ϕ.
- Then assumed the MFR have cylindrical crosssection
- Field inside MFR were modelled using observations at 1 AU.
- Accelerations were estimated using Lorentz force
- Relativistic converson were used into particle frame.
- Inside MFR its position and velocity were estimated in every 100 m travel.

Simulation of Particle Trajectory

- We used Cordinate system with origin at MFR center.
- It can be obtained from GSE by rotation R_Z by θ and R_Y by ϕ.
- Then assumed the MFR have cylindrical crosssection
- Field inside MFR were modelled using observations at 1 AU.
- Accelerations were estimated using Lorentz force
- Relativistic converson were used into particle frame.
- Inside MFR its position and velocity were estimated in every 100 m travel.
- We chose only particle that travel significant distance along axial direction

Simulation of Particle Trajectory

- We used Cordinate system with origin at MFR center.
- It can be obtained from GSE by rotation R_Z by θ and R_Y by ϕ.
- Then assumed the MFR have cylindrical crosssection
- Field inside MFR were modelled using observations at 1 AU.
- Accelerations were estimated using Lorentz force
- Relativistic converson were used into particle frame.
- Inside MFR its position and velocity were estimated in every 100 m travel.
- We chose only particle that travel significant distance along axial direction

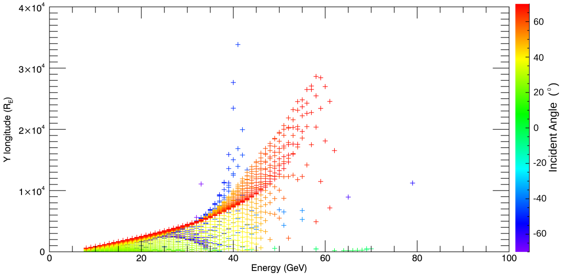

GCR guiding

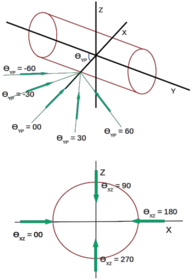
Z
X
Y
Θ = 90
Θ = 180
Θ = 00
Θ = 270
X

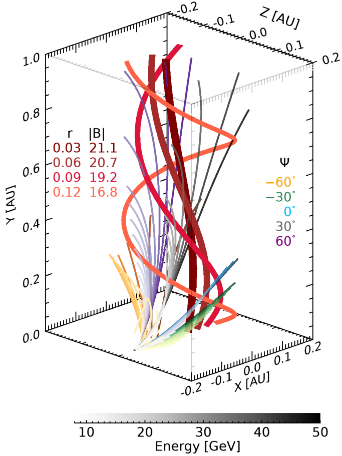
Z [AU]
X [AU]
Y [AU]
r |B|
0.03 21.1
0.06 20.7
0.09 19.2
0.12 16.8
Ψ
−60˚
−30˚
0˚
30˚
60˚
Energy [GeV]

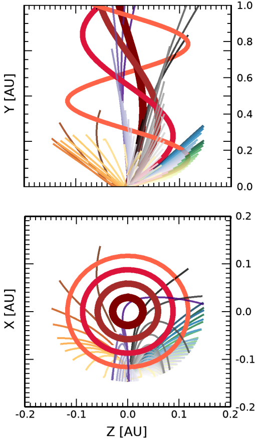
Y [AU]
X [AU]
Z [AU]

GCR guiding- Crossection view

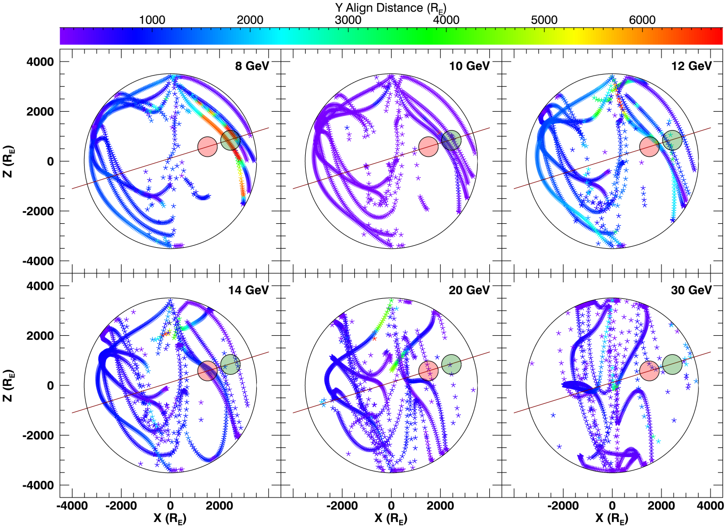

Coupling to HAWC direction

Assymtotic direction of HAWC, Estimated using IGRF12, and backtracing method.

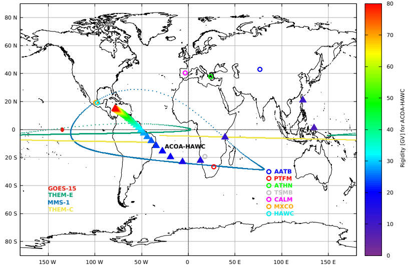

Coupling to HAWC direction

Assymtotic direction of HAWC, Estimated using IGRF12, and backtracing method.

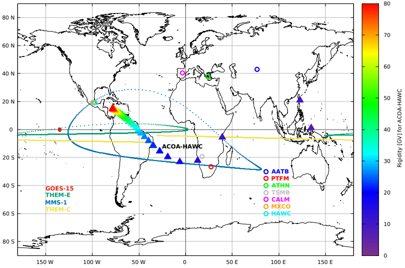

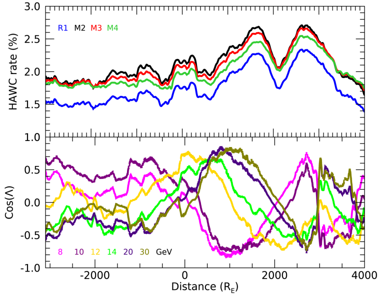

$$\cos(\Lambda) = \frac{\hat{N} \cdot \vec{B}}{|B|}.$$

Λ is the angle between assymtotic direction and the interplanetary magnetic field.

Other observations

Time difference as a function of geo-longitude of the observed decrease of rates

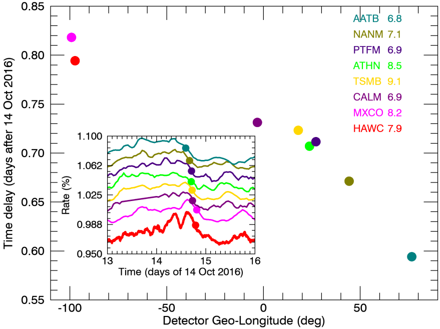

HAWC rate is scaled down by a factor of 30

Results

- The CME was associated with a very weak shock, which does not shield away the GCRs from getting into the fluxrope.

Results

- The CME was associated with a very weak shock, which does not shield away the GCRs from getting into the fluxrope.
- The MFR was with perfect magnetic topology and low density cavity, because of which the ram-pressure was lower than ambient solar wind.

Results

- The CME was associated with a very weak shock, which does not shield away the GCRs from getting into the fluxrope.
- The MFR was with perfect magnetic topology and low density cavity, because of which the ram-pressure was lower than ambient solar wind.
- The GCRs of low GeV energy were trapped inside the MFR and guided through the axis.

Results

- The CME was associated with a very weak shock, which does not shield away the GCRs from getting into the fluxrope.
- The MFR was with perfect magnetic topology and low density cavity, because of which the ram-pressure was lower than ambient solar wind.
- The GCRs of low GeV energy were trapped inside the MFR and guided through the axis.
- These particle were allowed to enter in to Earth's atmosphere while it was passing through MFR.

Results

- The CME was associated with a very weak shock, which does not shield away the GCRs from getting into the fluxrope.
- The MFR was with perfect magnetic topology and low density cavity, because of which the ram-pressure was lower than ambient solar wind.
- The GCRs of low GeV energy were trapped inside the MFR and guided through the axis.
- These particle were allowed to enter in to Earth's atmosphere while it was passing through MFR.
- The first enhancement observed in HAWC was dues to 14-30 GeV protons, where as second peak was due to 8-12 GeV protons.

Results

- The CME was associated with a very weak shock, which does not shield away the GCRs from getting into the fluxrope.
- The MFR was with perfect magnetic topology and low density cavity, because of which the ram-pressure was lower than ambient solar wind.
- The GCRs of low GeV energy were trapped inside the MFR and guided through the axis.
- These particle were allowed to enter in to Earth's atmosphere while it was passing through MFR.
- The first enhancement observed in HAWC was dues to 14-30 GeV protons, where as second peak was due to 8-12 GeV protons.
- First evidence of particle guiding inside a fluxrope.


Thank You..